Oblique anchoring at a free nematic surface

F.N. Braun, T.J. Sluckin, and E. Velasco*
Faculty of Mathematical Studies, University of Southampton, Southampton SO17 1BJ, United Kingdom

L. Mederos
Instituto de Ciencia de Materiales, Consejo Superior de Investigaciones Científicas, E-28049 Madrid, Spain
(Received 8 June 1995)

We generalize earlier density functional theories of the interface between an ordered nematic liquid crystal and its vapor to consider oblique anchoring. This is achieved by including a term with the symmetry of the electrostatic quadrupole in the model molecular interaction potential. As the bulk triple point of the liquid crystal is approached, the model exhibits the second-order oblique-to-homeotropic anchoring transition observed experimentally by Chiarelli *et al.* The result constitutes a thermodynamically consistent demonstration of this phenomenon using a microscopic theory. We plot the relevant anchoring phase diagrams, and compare them with constrained treatments of the density functional. By means of this comparison we assess to what extent the commonly adopted strategy of decoupling interfacial structure from anchoring is justified.

PACS number(s): 61.30.Cz, 61.30.Gd, 64.70.Md, 68.10.Cr

I. INTRODUCTION

The phenomenon of anchoring in liquid crystals has stimulated a great deal of experimental research over the last few decades, greatly motivated by the importance of the field to the development of liquid-crystal display devices. Anchoring is a generic term for the orientation of liquid crystals by a surface, dividing naturally into two categories: orientation of liquid-crystal molecules at a surface by a substrate potential, and spontaneous orientation of the molecules due to the bond-breaking symmetry of the surface. The free surface is particularly interesting in that anchoring properties may be regarded as exclusively driven by the latter mechanism.

The main focus in anchoring discussions is on the identification of an anchoring angle, defined as the nematic director orientation at the surface. An anchoring angle normal to the surface is known as homeotropic anchoring, while planar describes anchoring in the plane of the surface, and all intermediate anchoring orientations are classed as oblique. Terminology also exists for degenerate sets of anchoring angles, but is not needed for the present purpose. The reader is referred to Jérôme [1] for a full review of anchoring.

This paper consists in applying density functional theory to anchoring at the free surface. The relevant statistical mechanical system is that of the diffuse interface formed by the nematic phase of a liquid crystal in equilibrium with its vapor; a system that has been extensively studied using density functional theory. Initial work was carried out by Telo da Gama and co-workers [2,3] whose model predicted homeotropic and planar anchoring but was not sufficiently general to cover the oblique case. This corresponds well to experimental results for the cyano-biphenyls nCB ($n = 5, 7, 8$), which exhibit homeotropic alignment [4,5], and PAA (parazoxyanysole), which exhibits planar alignment [6]. However, more subtle anchoring behavior is observed in N-(4′-methoxybenzylidene)-4-(n-butyl)aniline (MBBA) and N-(4′-ethoxybenzylidene)-4-(n-butyl)aniline (EBBA). Chiarelli, Faetti, and Fronzoni [7] find a second-order oblique-to-homeotropic transition in both these cases, occurring close to the respective clearing points. While phenomenological studies exist to explain this effect [8,9], calculations have not yet been performed at the microscopic level within a thermodynamically consistent framework such as the density functional method.

The present study will begin in Sec. II with a description of the model based on that of Telo da Gama, discussing how this formalism may be generalized to allow obliquely tilted director configurations. In Sec. III we present numerical calculations that focus on the nature of the oblique-to-homeotropic anchoring transition. One of the advantages of the density functional model over phenomenological approaches is that it allows an appraisal of the role in determining the anchoring angle of other structural features at the surface, such as wetting properties and interfacial characteristic widths. In this spirit, the emphasis in discussing the calculated anchoring phase diagram will be on contrasting the equilibrium results with results obtained from two approximations designed to help elucidate this interplay. It is hoped that in doing so we provide an assessment of the validity of existing phenomenological studies [10,11] which implicitly decou-

*Present address: Departamento de Física de la Materia Condensada, Universidad Autónoma de Madrid, E-28049 Madrid, Spain.

ple the anchoring angle from other aspects of interfacial structure.

Finally, in Sec. IV we present some conclusions.

II. THE DENSITY FUNCTIONAL MODEL

Here we describe the main features of the density functional model prescribed by Telo da Gama in the context of the nematic-vapor interface, and introduce the necessary modifications for the oblique anchoring case. A number of recent, largely technical improvements, implemented in [12,14,15] will also be incorporated.

The model may be regarded as a generalization of the well-known Maier-Saupe theory [16] in that it is a mean-field approach. The system is characterized by the one-particle distribution function $\rho(\mathbf{r},\hat{\omega})$, where $\mathbf{r}$ is the position of a point in the material and $\hat{\omega}$ the molecular orientation. In density functional theory (see, e.g., Evans [17]), a grand potential functional $\Omega[\rho(\mathbf{r},\hat{\omega})]$ is constructed, and the equilibrium distribution is taken as that which minimizes the functional. We consider the form

$$\Omega[\rho(\mathbf{r},\hat{\omega})] = \int d\mathbf{r} f_{\mathrm{HC}}(\mathbf{r}) - \mu \int d\mathbf{r} d\hat{\omega} \rho(\mathbf{r},\hat{\omega}) + \frac{1}{2}\int\int d\mathbf{r} d\mathbf{r}' d\hat{\omega} d\hat{\omega}' \rho(\mathbf{r},\hat{\omega}) \times V_{\mathrm{att}}(\mathbf{r}-\mathbf{r}',\hat{\omega},\hat{\omega}')\rho(\mathbf{r}',\boldsymbol{\omega}'), \quad (1)$$

where μ is the chemical potential. Repulsive interactions in the model are incorporated by means of a hard core reference fluid, a hard sphere fluid, described in local-density approximation by the free-energy density

$$f_{\mathrm{HC}} = f_{\mathrm{ideal}} + \Delta f_{\mathrm{rep}}, \quad (2)$$

where the first term accounts for the free energy of the ideal gas limit, and the second term represents the excess free energy due to repulsive interactions between the molecules. We choose for the latter the Carnahan-Starling expression for hard spheres in our calculations, in line with [14,15].

The anisotropy of the attractive potential V_{att} is well formulated by expanding in spherical harmonics with respect to a laboratory-fixed frame of reference [3],

$$V_{\mathrm{att}}(\mathbf{r},\hat{\omega},\hat{\omega}') = \sum_{ll_1l_2} V_{ll_1l_2}(r) \sum_{m_1m_2m} C(ll_1l_2;m_1m_2m) \times Y_{l_1m_1}(\hat{\omega})Y_{l_2m_2}(\hat{\omega}')Y^*_{lm}(\hat{\mathbf{r}}). \quad (3)$$

Following [14,15], we choose Lennard-Jones forms for the components $V_{l_1l_2l}(r)$, with the Weeks-Chandler-Anderson modification at short distances:

$$V_{l_1l_2l}(r) = \epsilon_{l_1l_2l} v(r),$$

$$v(r) = \begin{cases} \left[\left(\frac{\sigma}{r}\right)^{12} - \left(\frac{\sigma}{r}\right)^{6}\right], & r > 2^{1/6}\sigma \\ -1/4, & r < 2^{1/6}\sigma, \end{cases} \quad (4)$$

where σ is the hard sphere diameter.

On truncating the expansion of Eq. (3) at $l = 2$ and using the addition theorem for spherical harmonics we obtain

$$V_{\mathrm{att}}(\mathbf{r},\hat{\omega},\hat{\omega}') = v(r)\{A + BP_2(\hat{\omega}\cdot\hat{\omega}') + C[P_2(\hat{\omega}\cdot\hat{\mathbf{r}}) + P_2(\hat{\omega}'\cdot\hat{\mathbf{r}})] + D\Gamma(\hat{\omega},\hat{\omega}',\hat{\mathbf{r}})\} \quad (5)$$

where P_2 denotes the second Legendre polynomial, and we have used the following definitions

$$A = \frac{\epsilon_{000}}{(4\pi)^{3/2}}, \qquad B = \frac{\sqrt{5}\epsilon_{220}}{(4\pi)^{3/2}},$$

$$C = \frac{5\epsilon_{202}}{(4\pi)^{3/2}}, \qquad D = \frac{15\epsilon_{224}}{\sqrt{70}(4\pi)^{3/2}}, \quad (6)$$

$$\Gamma(\hat{\omega},\hat{\omega}',\hat{\mathbf{r}}) = 1 - 5(\hat{\omega}\cdot\hat{\mathbf{r}})^2 - 5(\hat{\omega}'\cdot\hat{\mathbf{r}})^2 + 2(\hat{\omega}\cdot\hat{\omega}')^2 + 35(\hat{\omega}\cdot\hat{\mathbf{r}})^2(\hat{\omega}\cdot\hat{\mathbf{r}})^2 - 20(\hat{\omega}\cdot\hat{\mathbf{r}})(\hat{\omega}'\cdot\hat{\mathbf{r}})(\hat{\omega}\cdot\hat{\omega}') \; . \quad (7)$$

An additional contribution V_{222} will not be considered in this work.

The first three terms of Eq. (5), governed by A, B, and C, are the basic ingredients in studies of planar and homeotropic anchoring [3,12]. The B term is the usual Maier-Saupe term, while the C term couples the molecular orientation to the intermolecular vector $\mathbf{r}$, thus driving transitions between planar and homeotropic configurations.

The focus of the present work is the last term governed by D. This term has the symmetry of an electric quadrupole, although an electric quadrupole interaction would have a long-range behavior proportional to r^{-5}, and not r^{-6} as here. For D negative, however, the shape of this term more or less corresponds to an electric quadrupolar interaction between molecules all of which have electric quadrupoles of the same sign. For this reason we confine our discussion to negative D. Barbero and Durand [13] have connected tilted orientations at liquid-crystal interfaces and in the smectic-C phase to the phenomenon of order electricity, which is dependent on the existence of a quadrupolar intermolecular potential. This idea has been confirmed in a simple mean-field model by Tjipto-Margo and Sullivan [18] and by Teixeira and Sluckin [19]. We thus expect that competition between C and D will drive oblique anchoring effects.

A. Order parameters and tilt

Here we discuss how to obtain the relevant order parameters from the particle distribution function.

It is convenient to define the orientational distribution function, $f(\mathbf{r},\hat{\omega})$, as

$$\rho(\mathbf{r},\hat{\omega}) \equiv \rho(\mathbf{r}) f(\mathbf{r},\hat{\omega}), \tag{8}$$

where $\rho(\mathbf{r})$ denotes the one-particle density. In addition we define the z direction along the surface normal, and suppose spatial uniformity in the plane of the surface. The surface is in principle azimuthally symmetric. A tilted director breaks this symmetry. We shall suppose that the director remains in the x-z plane. The laboratory-fixed frame of reference is fixed by the usual Cartesian coordinate system. Thus, we write $\rho(\mathbf{r}) = \rho(z)$ and $f(\mathbf{r},\hat{\omega}) = f(z,\hat{\omega})$.

The ideal gas contribution to the free-energy density of the reference fluid Eq. (2) may now be divided into translational and rotational parts

$$\begin{aligned}\beta f_{\text{ideal}}(z) &= \int d\hat{\omega}\rho(\mathbf{r},\hat{\omega})[\ln\rho(\mathbf{r},\hat{\omega}) - 1] \\ &= \rho(z)[\ln\rho(z) - 1] - \rho(z)S_{\text{rot}}(z),\end{aligned} \tag{9}$$

where the local rotational entropy per particle is

$$S_{\text{rot}}(z) = -\int d\hat{\omega} f(z,\hat{\omega}) \ln 4\pi f(z,\hat{\omega}), \tag{10}$$

and $\beta = 1/k_B T$.

Nematic order may be characterized by moments of the orientational distribution $f(z,\hat{\omega})$, which has the advantage of yielding a set of scalar profiles in z. Allowing for biaxiality, the symmetry of our system gives rise to three such order parameters [2]:

$$\begin{aligned}\eta(z) &= \int d\hat{\omega} P_2(\cos\theta) f(z,\hat{\omega}), \\ \sigma(z) &= \int d\hat{\omega} \sin^2\theta \cos(2\phi) f(z,\hat{\omega}), \\ \nu(z) &= \int d\hat{\omega} \sin 2\theta \cos(\phi) f(z,\hat{\omega}),\end{aligned} \tag{11}$$

where θ and ϕ are the Euler coordinates in the laboratory-fixed frame of reference. For the case of obliquely tilted director configurations, these three profiles are not directly identifiable with uniaxial and biaxial order. We must first consider the tilt profile $\psi(z)$, defined as the z dependence of the director frame of reference with respect to the laboratory-fixed frame. A simple relation between the tilt and $\{\eta(z),\sigma(z),\nu(z)\}$ may be derived from the following rotation identities [20,21]:

$$\begin{aligned}\eta_d &= \frac{\eta}{2}(3\cos^2\psi - 1) + \frac{3\sigma}{4}\sin^2\psi + \frac{3\nu}{2}\sin\psi\cos\psi, \\ \sigma_d &= \eta\sin^2\psi + \frac{\sigma}{2}(1+\cos^2\psi) - \nu\sin\psi\cos\psi, \\ \nu_d &= -2\eta\sin\psi\cos\psi + \sigma\sin\psi\cos\psi + (2\cos^2\psi - 1)\nu \\ &= 0,\end{aligned} \tag{12}$$

where the subscript d denotes the director frame of reference and η_d and σ_d correspond, respectively, to uniaxial and biaxial order. Solving Eq. (12) for the tilt ψ, we obtain

$$\psi = \frac{1}{2}\arctan\frac{2\nu}{2\eta - \sigma}. \tag{13}$$

Thus we have a choice between the two equivalent sets of orientational profiles $\{\eta(z),\sigma(z),\nu(z)\}$ or $\{\eta_d(z),\sigma_d(z),\psi(z)\}$.

B. Numerical method

Either of the two sets of profiles discussed above may be used in solving the density functional problem. Choosing the laboratory-fixed order parameters, the free-energy density from attractive interactions per unit area of the interface may be written

$$\begin{aligned}f_{\text{att}}(z) = \rho(z)\int dz'\rho(z')\Big[&A\tilde{v}_{000}(z-z') + B\tilde{v}_{220}(z-z')\left(\eta(z)\eta(z') + \frac{3}{4}\sigma(z)\sigma(z') + \frac{3}{4}\nu(z)\nu(z')\right) \\ &+C\tilde{v}_{202}(z-z')\left[\eta(z)+\eta(z')\right] + D\tilde{v}_{224}(z-z')\left(6\eta(z)\eta(z') + \frac{3}{4}\sigma(z)\sigma(z') - 3\nu(z)\nu(z')\right)\Big],\end{aligned} \tag{14}$$

where $\tilde{v}_{l_1 l_2 l}(z)$ denotes the projection of the r dependence $v(r)$ of the respective spherical harmonic components along the z direction,

$$\tilde{v}_{l_1 l_2 l}(z) = \int d\mathbf{R} v(r) P_l(z/r), \tag{15}$$

with $\mathbf{r} = (\mathbf{R}, z)$.

This form is amenable to a multidimensional minimization technique such as the method of conjugate gradients [22] in which $\rho(z)$, $\eta(z)$, $\sigma(z)$, and $\nu(z)$ are discretized onto an N-point lattice along the z axis, i.e., $\rho_i = \rho(z_i)$, $\eta_i = \eta(z_i)$, etc., $z = hi$. In all our calculations we set $N = 300$, $h = 0.2\sigma$. The conjugate gradient tolerance level was between 10^{-4} and 10^{-3}. Equilibrium structure and thermodynamical properties are then obtained by minimizing the grand potential functional of Eq. (1) with respect to the resulting $4N$ variables. To this end it is necessary to express local rotational entropy of the molecules [Eq. (10)] in terms of the orientational order

parameters. The reader is referred elsewhere [14,15] for a discussion of this point. Expressions for the gradients $d\Omega/d\rho_i$, $d\Omega/d\eta_i$, etc., which are required by the conjugate gradient technique, are relatively straightforward to obtain.

Identifying the bulk nematic and vapor phases with $z \to \infty$ and $z \to -\infty$, respectively, the appropriate boundary conditions and the chemical potential are obtained by calculating bulk coexistence using the same lattice. This does not, however, define the boundary condition at the nematic side on the tilt, since the bulk free energy is rotationally invariant. We may choose either $d\psi/dz(\infty) = 0$ or $\psi(\infty)$ =const. The former is not easy to implement numerically, and so we must also minimize with respect to $\psi(\infty)$.

It remains to specify the initial guess for the system variables. The trial functions used in [3] are

$$\rho(z) = \frac{1}{2}(\rho_N + \rho_V) + \frac{1}{2}(\rho_N - \rho_V)\tanh\left(\frac{z - z_{NI}}{\xi_\rho}\right),$$

$$\eta_d(z) = \frac{\eta_{\text{bulk}}}{1 + \exp[(\Delta z + z_{NI} - z)/\xi_\eta]}, \tag{16}$$

where ρ_N and ρ_V are the densities of the bulk nematic and vapor phases, respectively, and η_{bulk} is the uniaxial order parameter in the bulk nematic phase. A dividing surface at z_{NI} pins the interface. Diffuseness of the interface is governed by ξ_ρ and ξ_η, representing interfacial widths associated with the $\rho(z)$ and $\eta_d(z)$ profiles, respectively. A depinning factor Δz defines the relative shift between the two profiles, and may be regarded as an indicator of wetting by the isotropic phase.

Biaxiality is neglected in the initial guess (i.e., $\sigma_d = 0$), but an initial tilt profile is clearly necessary, and so we adopt the simplest option of uniform tilt commensurate with the boundary condition. Note, however, that we have specified the orientational profiles in the director frame of reference. Recalling that we chose to work in the laboratory-fixed frame, the η_d profile must first be rotated with respect to the tilt to obtain $\{\eta(z), \sigma(z), \nu(z)\}$ before the functional can be evaluated.

Numerical efficiency can be enhanced by preceding the $4N$-dimensional minimization procedure with a constrained minimization with respect to the parameters governing the initial profiles. This naturally leads us to speculate that these parameters might in fact turn out to be essentially sufficient for an accurate description of the anchoring properties. If that were the case, the cumbersome machinery needed for $4N$-dimensional minimization would be superfluous. The differences between the predictions of the two theories are small but nevertheless noticeable, as we shall see in the results below. The restricted parameter theory provides extremely useful physical insight. The precise location of the interface z_{NI} is of course arbitrary since it describes a Goldstone mode. The remaining three free parameters ξ_ρ, ξ_η, and Δz describe the interfacial structure rather well. The difference between minimizing with respect to $4N$ as opposed to three variables manifests itself in a number of relatively minor details in the order parameter profiles. The incomplete minimization of the free energy has relatively minor implications on the anchoring phase diagram.

III. THE OBLIQUE-HOMEOTROPIC ANCHORING TRANSITION

This section begins by introducing appropriate rescalings and setting system parameters. Calculated equilibrium profiles are then discussed before going on to discuss the anchoring angle and surface tension in the vicinity of the anchoring transition, and finally the associated anchoring phase diagrams. We shall compare our results with those of two approximation schemes that give useful reference points. These are (a) the so-called Fowler approximation, which is analytical, and (b) the approximation based on the numerical trial functions discussed above.

A reduced temperature scale is set using the parameter A in Eq. (14) according to $T^* = k_BT/A$, making it convenient to also rescale B, C, and D with $\bar{B} = B/A$, $\bar{C} = C/A$, $\bar{D} = D/A$.

The thermodynamic quantity that will be of greatest interest in the following is the surface free energy $\gamma = (\Omega - \Omega_{\text{bulk}})/\text{area}$, or the corresponding dimensionless quantity $\bar{\gamma} = \gamma\sigma^2/k_BT$. We remark that this is probably what is measured in surface tension experiments in these fluids. The surface tension, properly defined, is a tensor quantity.

Henceforth the bar and suffix notations used in all of the above rescalings will be dropped, and the rescaling assumed.

Following [2], B is fixed at 0.3, and consequently the bulk phase diagram of the model is similar to that of the original Telo da Gama model, i.e., independent of C and D [3]. The bulk phase diagram exhibits the nematic, isotropic, and vapor phases with a triple point at $T = 0.2018$ [14].

In examining interfacial properties, the parameters C, D, and T define the relevant phase space. With $D = 0$, negative C induces uniform zero tilt, i.e., homeotropic anchoring [3]. We shall consider here negative C, which favors planar anchoring, and would forbid oblique to homeotropic transitions. Positive D is not relevant as discussed in the last section. Our analysis is thus restricted to the domain of negative C and negative D.

A significant part of this domain is associated with oblique anchoring. We show an example in Fig. 1 of the solution of the density functional for a combination of C and D, which exhibits an obliquely tilted director configuration. A section of the equilibrium interface profiles (in the director frame of reference) is plotted for $T = 0.2$, $D = -0.32$, $C = -0.1$. The bulk tilt angle that corresponds to the equilibrium solution is 22.53°.

The $\rho(z)$ and $\eta_d(z)$ profiles show the expected similarity with results obtained by Thurtell, Telo da Gama, and Gubbins [3] for the homeotropic and planar anchoring

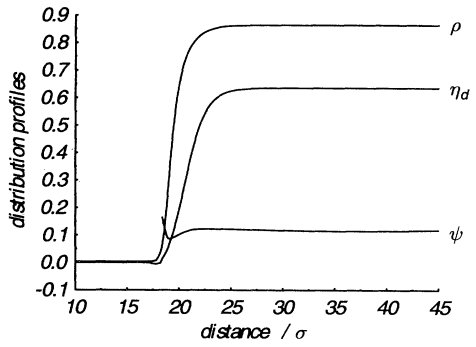

FIG. 1. The interface profiles at $T = 0.2$, $C = -0.1$, $D = -0.32$ in the director frame of reference. The resolution of 0.2σ (where σ is the hard core radius) is slightly too low to show all of the $\eta_d(z)$ fine structure.

cases, notably the low-amplitude fine structure in $\eta_d(z)$ close to z_{NI}. We have not shown the biaxial fine structure, which is negligible. The new feature in our case is the tilt profile $\psi(z)$ which, by contrast with the planar and homeotropic cases, is nonuniform at the interface.

An immediate concern now lies in how to define an anchoring angle ψ_A. The question is not a trivial one (see, e.g., [19]), but in the interests of avoiding numerical complications we choose in the following to define it as the bulk tilt. That is, the free surface anchoring angle in the numerical calculations is interpreted as the boundary condition on the tilt that minimizes the surface tension.

Using this definition, Fig. 2 shows an example of the oblique to homeotropic transition, with ψ_A plotted against temperature T for fixed $D = -0.32$ and $C = -0.15$. We see that as the transition temperature is approached, ψ_A goes to zero continuously, defining a second-order transition (note that, in the figure, the dashed segment represents an extrapolation up to the estimated critical temperature).

Parsons [8] long ago proposed a Landau form to describe the MBBA anchoring transition, the relevant scalar order parameter in the anchoring context being

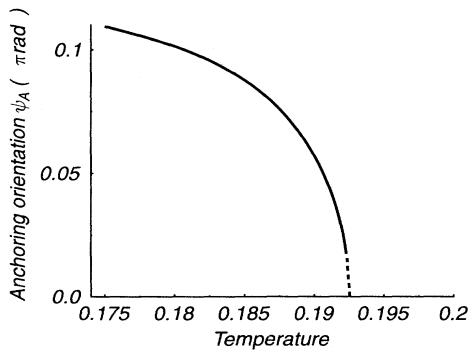

FIG. 2. Evolution of the anchoring orientation vs temperature for fixed $C = -0.15$, $D = -0.32$.

ψ_A. The mean-field 1/2 exponent is clearly in evidence in the limit $T \to T_{\rm OH}$ where $T_{\rm OH}$ is the oblique-to-homeotropic anchoring transition temperature. Thus our results are consistent with the Landau form, but only close to $T_{\rm OH}$, as indeed is the case experimentally [7].

Before discussing the surface tension, let us examine the two approximation schemes with which we compare the equilibrium results.

A. The Fowler approximation

This strategy [23] has been adopted in many phenomenological studies of anchoring and wetting at nematic surfaces (e.g., [10,21]). We follow Refs. [18,19] in considering it at the microscopic level where its strength lies in the fact that it makes evaluation of the surface tension analytically tractable, yielding an explicit Landau-type expression for its dependence on the model parameters. In effect, the result constitutes a microscopically derived phenomenology.

The approximation consists in simply constraining the interfacial structure to a Heaviside step function, thus neglecting interfacial width and structure (the vapor density is also neglected):

$$\rho(z) = \begin{cases} \rho_N, & z > z_{NI} \\ 0, & z < z_{NI}, \end{cases}$$
$$\eta_d(z) = \begin{cases} \eta_{\rm bulk}, & z > z_{NI} \\ 0, & z < z_{NI}. \end{cases} \tag{17}$$

When this constraint is relaxed, as in the mean-field treatment of density functional theory, the surface tension will of course be lower. However, a direct comparison between the Fowler approximation and equilibrium properties calculated from density functional theory, as we propose to include here, has not yet been carried out for our system of interest.

In the Fowler approximation, all contributions to the functional of Eq. (1) cancel [19] except for the surface free energy from attractive interactions. The surface tension γ is then obtained from Eq. (14) alone according to

$$\gamma = \int_{z_{NI}}^{\infty} dz \{ f_{\rm att}(z) - f_{\rm att}(\infty) \}, \tag{18}$$

giving for uniform tilt ψ

$$\gamma = \frac{\rho_N^2}{T} \{ (1 + B\eta_{\rm bulk}^2) k_0 + C\eta_{\rm bulk} k_2 P_2(\cos\psi) + D\eta_{\rm bulk}^2 k_4 P_4(\cos\psi) \}, \tag{19}$$

where P_2 and P_4 are the Legendre polymonials of orders two and four, and to three significant figures, we calculate $k_0 = 0.701$, $k_2 = 0.378$, $k_4 = -0.174$. Except for these model specific constants, Eq. (19) is identical to the expression derived in [19].

For comparison with Parsons's theory, the corresponding Landau form is

$$\Delta\gamma(\sin\psi) = \gamma(0) - \gamma(\sin\psi)$$
$$= \alpha(T)[C - C_{\rm OH}^{\rm Fowler}(T,D)]\sin^2\psi + \beta(T,D)\sin^4\psi, \quad (20)$$

where the Landau coefficients are given by

$$\alpha(T) = -\frac{3}{2T}k_2\rho_N^2\eta_{\rm bulk},$$

$$\beta(T,D) = \frac{35D}{8T}k_4\rho_N^2\eta_{\rm bulk}^2, \quad (21)$$

and a surface of second order oblique to homeotropic transitions is defined according to

$$C_{\rm OH}^{\rm Fowler}(T,D) = -\frac{10Dk_4\eta_{\rm bulk}}{3k_2}. \quad (22)$$

For oblique anchoring (i.e., $D < 0$, $C > C_{\rm OH}^{\rm Fowler}$) we have from Eqs. (20) – (22)

$$\sin^2\psi_A^{\rm Fowler} = \frac{4}{7} + \frac{6}{35\eta}\frac{k_2}{k_4}\frac{C}{D}. \quad (23)$$

In the domain of negative C, the quadrupolar symmetry of the V_{224} term enforces an upper limit,

$$\lim_{D\to-\infty}\psi_A^{\rm Fowler} = \arcsin\sqrt{4/7}, \quad (24)$$

i.e., the minimum of $P_4(\cos\psi)$.

In order to describe in more detail the interfacial structure we use the interfacial characteristic lengths ξ_ρ, ξ_η, and Δz introduced in the last section. Constraining the density functional solution to these forms, we obtain an approximation intermediate between the Fowler approximation and the unconstrained equilibrium solution. We shall refer to these results as the "parameter constrained minimization" (PCM) solution.

B. Surface tension and anchoring phase diagram

Here we propose to compare the equilibrium anchoring properties from proper minimization of the density functional (which we shall refer to as "equilibrium") with the two approximation schemes introduced above.

Figure 3 illustrates the case $C = -0.17$, $D = -0.32$. At the top, the calculated PCM and Fowler [from Eq. (23)] anchoring angles are contrasted. The equilibrium oblique-to-homeotropic transition temperature is at $T_{\rm OH}^{\rm Eq} \approx 0.18$, significantly removed from the PCM result $T_{\rm OH}^{\rm PCM} \approx 0.1925$. The Fowler approximation exhibits no transition for these parameters, and evidently considerably overestimates the anchoring angle.

Associated with the $(T-T_{\rm OH})^{0.5}$ dependence of the anchoring angle near the transition, one expects from the Landau form that $\Delta\gamma(\psi_A) = \gamma(0) - \gamma(\psi_A)$ will exhibit $(T - T_{\rm OH})^2$ dependence. This is demonstrated in the middle part of the figure, and might be expected to give rise to an anomaly in the surface tension that would constitute a noticable signature of the anchoring transition. However, comparison with the PCM surface tension in the bottom part of the figure reveals that the order of magnitude of the anomaly is too small for it to be discernible in the general surface tension trend.

The depinning factor Δz is a measure of the width of an isotropic fluid interfacial layer. The Fowler approximation assumes $\Delta z = 0$, and may be expected to be inaccurate if Δz becomes large. For the value of C used here, $\Delta z(T)$ diverges as the isotropic-nematic transition is approached; this is known as wetting of the interface by the isotropic phase. This hypothesis may thus be tested. Comparison with the plotted surface tensions, however, does not seem to show that the Fowler approximation is

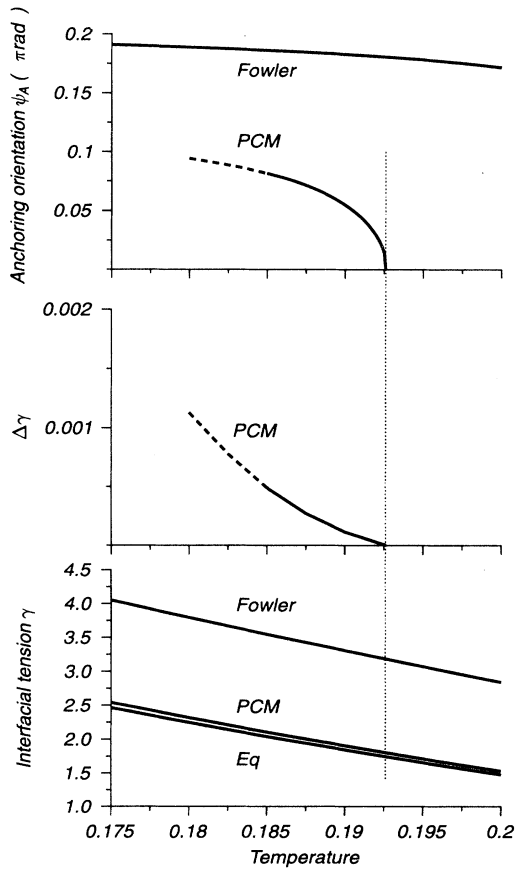

FIG. 3. Surface tension and associated anchoring behavior for $C = -0.17$, $D = -0.32$. The bottom part compares the equilibrium surface tension with the PCM and Fowler approximations. The oblique-to-homeotropic anchoring transition occurs at $T \approx 0.18$ in the equilibrium (Eq) case, and $T \approx 0.1925$ in the PCM approximation. The latter is marked by the dotted line. The middle part indicates the order of magnitude of the surface tension anomaly associated with the anchoring transition, seen to have no appreciable effect on the general trends of the lower part. The anchoring angle in the Fowler and PCM approximations is shown at the top. Note that the Fowler approximation predicts *no* transition for this choice of parameters.

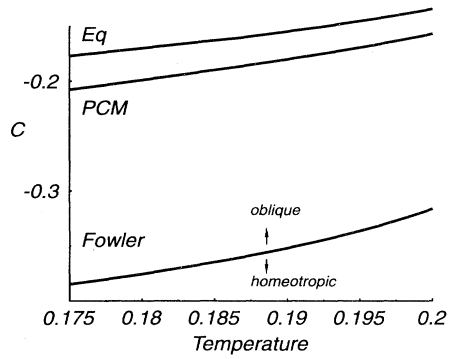

FIG. 4. Projection of the anchoring phase diagram in the T-C plane for fixed $D = -0.32$.

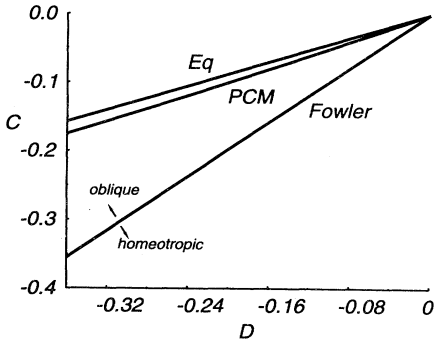

FIG. 6. Projection of the anchoring phase diagram in the D-C plane for fixed temperature $T = 0.2$.

appreciably worse close to the nematic-isotropic transition than elsewhere.

In Fig. 4 we plot the anchoring phase diagram for fixed $D = -0.32$. It is instructive to compare this with the behavior of the three interfacial lengths ξ_ρ, ξ_η, and Δz calculated in the PCM approximation. As the triple point is approached, we are again able to judge how structural changes at the interface affect the Fowler result. The three interfacial lengths along the coexistence line of Fig. 4 are plotted in Fig. 5. Each is a monotonic increasing function of temperature, reflecting the fact that the Fowler approximation is exact in the unphysical limit of $T = 0$, becoming progressively more disparate at higher temperatures. As the bulk triple point is approached, Δz increases more steeply, reflecting the isotropic wetting property, but it is somewhat surprising that, as for the surface tension, the Fowler and equilibrium anchoring coexistence curves of Fig. 4 show no apparent response. Thus, the diagram allows us to assert that the Clausius-Clapeyron-type expression for the gradient of the anchoring coexistence is reasonably accurate in the Fowler approximation, i.e., from Eq. (22)

$$\frac{dC_{\rm OH}^{\rm Eq}}{dT} \approx \frac{dC_{\rm OH}^{\rm Fowler}}{dT} = -\frac{10Dk_4}{3k_2}\frac{d\eta_{\rm bulk}}{dT}. \qquad (25)$$

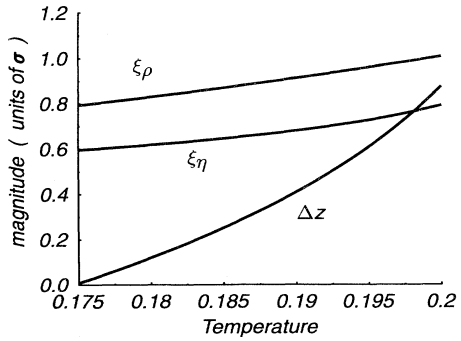

FIG. 5. Temperature dependence of the interfacial characteristic lengths Δz, ξ_η, and ξ_ρ along the oblique-homeotropic coexistence line, at constant $D = -0.32$.

Finally, we consider the projection of the anchoring phase diagram in the C-D plane, shown in Fig. 6 for constant $T = 0.2$ (i.e., near the triple point). All three curves exhibit linear dependence upon D as predicted by the Fowler approximation Eq. (22).

IV. CONCLUSION

We have used density functional theory to give a thermodynamically consistent account of oblique anchoring at the free nematic-vapor interface and the associated oblique-to-homeotropic transition.

Anchoring at the free surface presents a complex array of competing intermolecular forces, which have been well debated (see, e.g., Osipov and Hess [24]). Our study does not bring any revelations to this forum, and in fact the model used, a hard sphere fluid in an orientationally coupled mean-field Lennard-Jones potential, is clearly rather overidealized. We have, however, in addition to producing quantitative results, placed particular emphasis on a number of interfacial structural characteristics and their role in defining anchoring properties. This emphasis is of use in assessing various phenomenological assumptions made in the literature.

In summary, we find that in spite of the expected quantitative disparity, the assumption of a sharp interface as in the Fowler approximation leads to correct qualitative trends. In particular we find that oblique-homeotropic anchoring coexistence is second order and is well described by the Fowler result $C_{\rm OH} \propto D\eta(T)$. That is, the effect of neglecting surface structure is essentially only manifest in the constants of proportionality of this expression. A feature inherent to the Fowler approximation is that it ignores wetting properties, which we find seem to play a negligible part in determining the anchoring angle. Interestingly, Martin del Rio *et al.* [25] find, in a parallel calculation to ours, but in a different parameter range, a first-order, rather than a continuous, anchoring transition. This result seems peculiar, is not what the Landau theory would at first sight lead one to expect, and clearly merits further investigation.

ACKNOWLEDGMENTS

This work was partly supported by the "Acciones Integradas" Grant No. HB141 jointly financed by the British Council and the Ministerio de Educación y Ciencia of Spain. Financial support by (UK) EPSRC under Grant No. GR/H68352 and DGICYT PB91-0090 (Spain) is also gratefully acknowledged. We are grateful to the authors of Ref. [25] for a preprint of their paper.

[1] B. Jérôme, Rep. Prog. Phys. **54**, 391 (1991).
[2] M.M. Telo da Gama, Mol. Phys. **52**, 585 (1984).
[3] J.H. Thurtell, M.M. Telo da Gama, and K.E. Gubbins, Mol. Phys. **54**, 321 (1985).
[4] J.E. Proust and L. Ter-Minassian-Saraga, J. Phys. (Paris), Colloq. **40**, C3-490 (1979).
[5] D. Beaglehole, Mol. Cryst. Liq. Cryst. **89**, 319 (1982).
[6] M.A. Bouchiat and D. Langevin-Cruchon, Phys. Lett. **34A**, 331 (1971).
[7] P. Chiarelli, S. Faetti, and L. Fronzoni, J. Phys. (Paris) **44**, 1061 (1983).
[8] J.D. Parsons, Phys. Rev. Lett. **41**, 877 (1978).
[9] H. Mada, Mol. Cryst. Liq. Cryst. **53**, 127 (1979).
[10] T.J. Sluckin and A. Poniewierski, in *Fluid Interfacial Phenomena*, edited by C.A. Croxton (John Wiley, Chichester, 1986).
[11] P.I.C. Teixeira, T.J. Sluckin, and D.E. Sullivan, Liq. Cryst. **14**, 1243 (1993).
[12] B. Tjipto-Margo, A.K. Sen, L. Mederos, and D.E. Sullivan, Mol. Phys. **67**, 601 (1989).
[13] G. Barbero and G. Durand, Mol. Cryst. Liq. Cryst. **179**, 57 (1990).
[14] L. Mederos and D.E. Sullivan, Phys. Rev. A **39**, 854 (1989).
[15] L. Mederos and D.E. Sullivan, Phys. Rev. A **46**, 7700 (1992).
[16] W. Maier and A. Saupe, Z. Naturforsch. **13a**, 564 (1958).
[17] R. Evans, in *Fundamentals of Inhomogeneous Fluids*, edited by D. Henderson (Marcel Dekker, New York, 1992).
[18] B. Tjipto-Margo and D.E. Sullivan, J. Chem. Phys. **88**, 6620 (1988).
[19] P.I.C. Teixeira and T.J. Sluckin, J. Chem. Phys. **97**, 1498 (1992).
[20] C.G. Gray and K.E. Gubbins, *Theory of Molecular Fluids*, Vol. 1 (Clarendon Press, Oxford, 1984).
[21] A.K. Sen and D.E. Sullivan, Phys. Rev. A **35**, 1391 (1987).
[22] W.H. Press, B.P. Flannery, S.A. Teukolsky, and W.T. Vetterling, *Numerical Recipes: The Art of Scientific Computing* (Cambridge University Press, Cambridge, 1986).
[23] R.H. Fowler, Proc. R. Soc. London A **159**, 229 (1937).
[24] M.A. Osipov and S. Hess, J. Chem. Phys. **99**, 4181 (1993).
[25] E. Martin del Rio, M.M. Telo da Gama, E. de Miguel, and L. Rull, Phys. Rev. E **52**, 5028 (1995).